Thermal stability of the passive film formed on 316L stainless steel surface studied by ToF-SIMS

Luntao Wang, Antoine Seyeux, Philippe Marcus

Preprint accepted for publication in Corrosion Science

DOI: 10.1016/j.corsci.2019.108395

Thermal stability of the passive film formed on 316L stainless steel surface studied by ToF-SIMS

Luntao Wang, Antoine Seyeux, Philippe Marcus*

Chimie ParisTech-CNRS, PSL Research University, Institut de Recherche de Chimie Paris (IRCP), Physical Chemistry of Surfaces Group, 11 rue Pierre et Marie Curie, 75005 Paris, France

Abstract: The modifications of the passive film formed on 316L stainless steel surface during stepwise heating in ultra-high vacuum up to 300°C have been studied *in situ* by ToF-SIMS. The pre-formed passive film (in 0.05M H_2SO_4) has a bilayer structure, comprising Fe-rich, Mo-rich (outer) and Cr-rich (inner) layers. Below 100°C, the passive film is stable. At 100°C - 250°C, dehydroxylation and dehydration is observed. Above 250°C, the main modification in the film is formation of chromium oxide at the expense of oxidized iron. At higher temperature, thicker Cr-rich inner layer with sharper inner/outer oxide interface is formed.

Keywords: Stainless steel; Passive film; Thermal stability; ToF-SIMS

Introduction

Stainless steels are employed in a wide range of technical applications due to the formation of a protective surface oxide layer, that can provide high corrosion resistance of the material in aggressive environments [1, 2]. The passive films formed on stainless steel surfaces, typically a few nanometres thick at room temperature, are known to be duplex with an outer layer rich in iron oxide while the inner layer is enriched in chromium oxide [3, 4]. The corrosion resistance of the surface depends mainly on the chromium rich inner oxide, which serves as a barrier against the attack of aggressive ions from the environment [5, 6].

The formation of oxide film on the stainless steel surface at different temperatures has been widely studied. The oxidation temperature and the oxygen pressure are the two key factors influencing the oxidation rate and the composition of the oxide film on SS alloys. Oxidation of SS surface in air at most temperatures (temperatures lower than 800°C), leads to the formation of a duplex oxide layer, consisting of an outer iron oxide and an inner chromium rich layer [7, 8]. Under reduced oxygen partial pressures (lower than 10^{-3} mbar), at oxidation temperatures above 800°C, chromium oxide is the predominant layer on the stainless steel surface [9, 10], while for the oxide films formed at temperatures lower than 400°C, both the iron and chromium oxide were reported to grow on the SS surfaces [11-14].

Heating the SS at high temperatures in vacuum, may lead to modifications of chemical composition and structure in the alloy at the metal/oxide interface, such as phase transformation as already shown in the

Corresponding author:

E-mail address: philippe.marcus@chimieparistech.psl.eu (Philippe Marcus).

literature [15, 16]. Many phenomena, including diffusion, selective oxidation and evaporation of elements, are ongoing in the process of vacuum annealing of SS [17, 18]. It is well known that the vacuum annealing for stainless steel at high temperatures (above 1000°C) will produce a marked chromium depletion zone in the alloy surface under the oxide film because the selective evaporation rate is much faster than the bulk diffusion rate of chromium [18, 19]. For vacuum annealing of SS at intermediate temperatures [17, 20], about 400°C to 800°C, the evaporation rate of chromium oxidized at the surface is strongly reduced, and a strong chromium enrichment could be observed in the alloy surface under the oxide film. Studies of vacuum annealing of stainless steel, especially under ultra-high vacuum (pressure lower than 10^{-9} mbar), at relatively low temperature (lower than 300°C) are still under discussion.

Native oxide films, formed in air on stainless steel surfaces, have been studied in the past, especially thanks to UHV techniques like XPS and ToF-SIMS [2, 21-24]. Among these studies, very few have focused on the thermal stability of native oxide films during annealing under UHV[25-27]. Asami et al. [25] have used XPS spectroscopy to study the modifications of the native oxide film for a series of Fe-Cr alloys by UHV annealing up to 380°C. When the temperature is higher than 300°C, the authors showed the iron oxide reduction and the modification of the chromium oxidation state in the oxide film. Castle et al. [26] used the energy loss features within XPS spectra to study the oxidation and subsequent vacuum annealing of an Fe/Cr alloy at 200-300°C. An iron oxide reduction and chromium oxide formation was observed. Recent *in situ* measurements, performed by Bouheida et al. [27] on Fe-12Cr alloy, show that annealing in UHV with a thermal ramp rate of 2°C/min up to 550°C, leads to iron oxide reduction due to chromium oxidation. Although XPS can provide information on composition changes after heat treatment, the evolution of the oxide film structure is not obtained with XPS after set temperature. ToF-SIMS is a promising way to study the thermal stability of the oxide structure during the stepwise heating.

The aim of the present work was to investigate the thermal stability and the modification of pre-formed passive films on 316L stainless steel up to 300°C in ultra-high vacuum (UHV). To this end, 316L SS were electrochemically passivated in H_2SO_4 and then annealed in UHV by increasing step by step the temperature, from room temperature up to 300°C. The stability of the passive oxide film has been monitored *in situ* during heating, and modifications of the composition and structure of the oxide films have been analyzed by ToF-SIMS.

Experimental

Sample preparation

A Fe-19Cr-13Ni-2.7Mo (wt%) polycrystalline sample was used. The samples were mechanically polished down to 0.25μm with diamond paste and then washed with acetone, ethanol and water in ultrasonic bath for 10 mins. The samples were then dried in compressed air.

A Gamry electrochemical workstation was used for electrochemical experiments. The electrochemical passivation was performed with a standard three-electrode configuration with an Au counter electrode and a saturated calomel electrode as the reference electrode. The electrolyte was 0.05M H_2SO_4 prepared with ultrapure chemicals (VWR®) and Millipore® water. Before measurement, the solution was deaerated by Ar bubbling for 30 minutes.

ToF-SIMS investigation

ToF-SIMS depth profiles were obtained using a ToF-SIMS 5 spectrometer (IONTOF GmbH - Germany). The spectrometer was run at an operating pressure of 10^{-9} mbar. The total primary ion flux was less than 10^{12} ions*cm^{-2} ensuring static conditions. A pulsed 25 keV Bi^+ primary ion source was employed for analysis, delivering 1.2 pA current over a 100 × 100 μm^2 area. High current bunched mode was used in order to get high mass resolution (ΔM/M ~10 000). Depth profiling was carried out by interlacing secondary ion analysis with sputtering using a 0.5 keV Cs^+ sputter beam giving a 17 nA target current over a 300 × 300 μm^2 area. Both Bi^+ and Cs^+ ion beams were impinging the sample surface at an angle of 45° and were aligned in such a way that the analyzed ions were taken from the center of the sputtered crater.

Data acquisition and post-processing were performed using the Ion-Spec software. The exact mass values of at least 5 known species were used to calibrate the data acquired in the negative ion mode.

Species	Characteristic ion
Hydroxide	$(OH)_2^-$
Metallic Fe	$^{56}Fe_2^-$
Metallic Ni	$^{58}Ni_2^-$
Iron oxide	$^{56}FeO_2^-$
Chromium oxide	$^{53}CrO_2^-$
Molybdenum oxide	$^{98}MoO_3^-$

Table 1. ToF-SIMS characteristic ions used to characterize the composition and structure of the oxide film formed on 316L SS

ToF-SIMS depth profiles were used to determine the composition and structure of the passive film, and to study its thermal stability. The characteristic ions were selected as shown in Table 1. It should be noted that the selected ions do not reflect the real stoichiometry of the species constituting the sample,

but are the appropriate markers of the studied species. Since ToF-SIMS is a non-quantitative technique (due to strong matrix effect on ion emission), the intensity of the plotted ions in the depth profiles cannot be compared directly and do not reflect the concentrations of the associated species in the substrate. However, variations of a single signal reflect in depth variations of the concentration. The depth profiles are plotted versus the sputtering time, and the sputtering time directly translates into oxide thickness. The oxide sputtering rate was determined by measuring, with a mechanical profilometer (Dektak 150, Veeco, Veeco-Instrument Europe, Dourdan, France), the depth of various craters after depth profiling. Assuming a similar oxide composition and density, a 0.04 nm/s sputtering rate was measured.

Results and discussion

Passive film formation and analysis

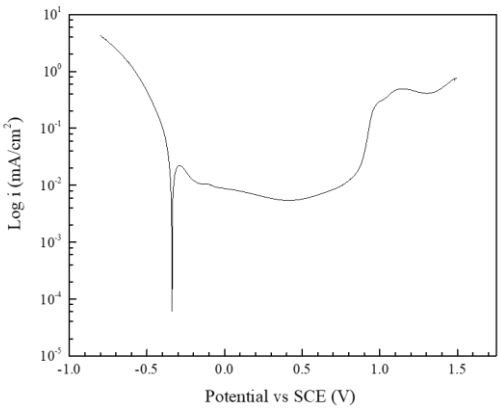

Fig.1 Polarization curve of the 316L SS in 0.05M H_2SO_4 with a scan rate of 1mV/s

Figure 1 shows the polarization curve obtained on 316L stainless steel in 0.05M H_2SO_4 aqueous solution with a scan rate of 1mV/s. Within the passive range (-0.1 ~ 0.8V/SCE), the lowest current is obtained at 0.4V/SCE, corresponding to the lowest dissolution rate of metallic ions in the solution. The oxide film formed at this potential shows the highest corrosion resistance. Maurice et al. have already demonstrated that the strong enrichment in chromium in the passive film formed in sulphuric acid, compared to the native oxide, is the result of the extremely low dissolution rate of Cr(III) oxide compared to the one of Fe(II)/Fe(III) oxides[21]. In this study, a static polarization potential (0.4V/SCE) was applied on the 316L SS for 1h in 0.05M H_2SO_4 aqueous solution to obtain a protective passive film on the sample surface.

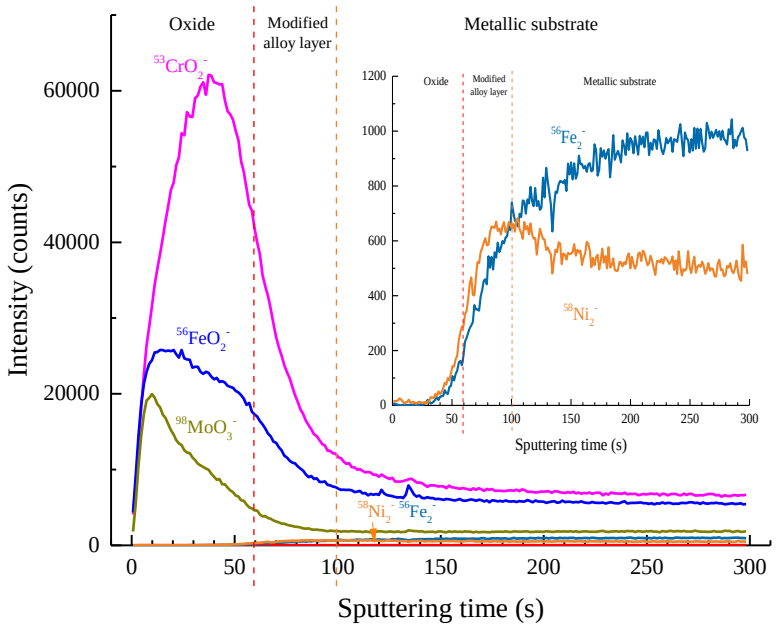

Fig.2 ToF-SIMS depth profiles of the passive film formed on 316L SS surface in 0.05M H_2SO_4(aq) at 0.4V/SCE for 1h. The colour lines mark the limits between oxide film, modified alloy layer and metallic substrate region

Figure 2 shows the ToF-SIMS negative ion depth profiles for the passive film formed in 0.05M H_2SO_4(aq) at 0.4V/SCE for 1h on the 316L SS. To study the thermal stability of the electrochemically pre-formed oxide film, the position of the metal/oxide interface on the ToF-SIMS depth profiles is crucial to extract the structure and composition of the oxide. The $^{53}CrO_2^-$ ion profile is used to define the oxide film region (ending at 80% of the maximum intensity of the depth profile) due to the duplex structure of the film with chromium enriched inner layer, and the $^{56}Fe_2^-$ ion profile is used to define the metallic region (starting at 80% of the intensity plateau). An intermediate region is determined in Fig.2 from 60s to 100s of sputtering. This region characterized by a hump in the $^{58}Ni_2^-$ signal, is assigned to a modified alloy layer under the oxide film in the vicinity of the oxide-metal interface. In this intermediate region, the progressive increase of the $^{56}Fe_2^-$ signal indicates, in contrast with the $^{58}Ni_2^-$ signal, a depletion in metallic Fe gradually disappearing. Thus, the alloy is enriched in Ni and depleted in Fe close to the metal/oxide interface.

Focusing on the $^{56}FeO_2^-$ and $^{98}MoO_3^-$ signals, the depth profile shows that their maxima are located in the outer part of the passive film and they decrease slowly through the oxide film region. Oxidized Fe and Mo are therefore mainly located in the outer part of the film, although they are also present in the inner oxide. The $^{53}CrO_2^-$ profile exhibits a maximum intensity in the inner part of the film. Oxidized chromium is thus preferentially located in the inner part, close to the metal/oxide interface. The $^{58}NiO_2^-$

ion is not plotted in Fig.2, since its intensity is too low, meaning that Ni oxide is present only as traces in the oxide film.

The model for the composition of passive film

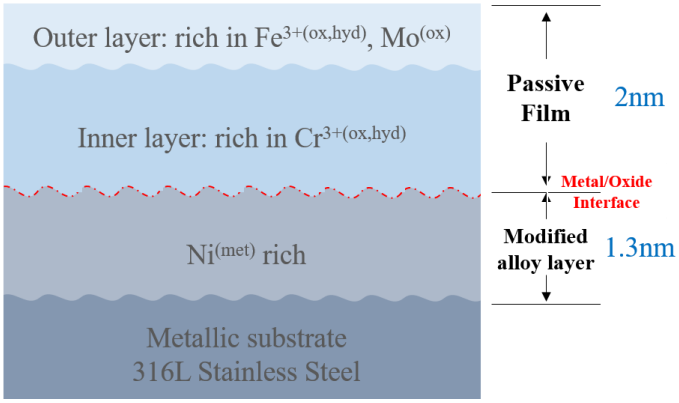

Fig.3 The model for the passive film formed on 316L SS surface in 0.05M H_2SO_4(aq) at 0.4V/SCE for 1h

Based on the ToF-SIMS depth profiles data, a model for the passive film and the alloy underneath the oxide is presented in Fig.3. In the model, it is considered that the passive film formed electrochemically is duplex with iron and chromium mainly in the outer and inner layers, respectively. Molybdenum oxide is mainly located in the outer part of the film. Nickel oxide is present only at trace amount. In a modified interfacial alloy layer, metallic nickel is enriched, compared to the metallic substrate. The model also suggests that the interfaces are not sharp.

Thermal stability of the passive film

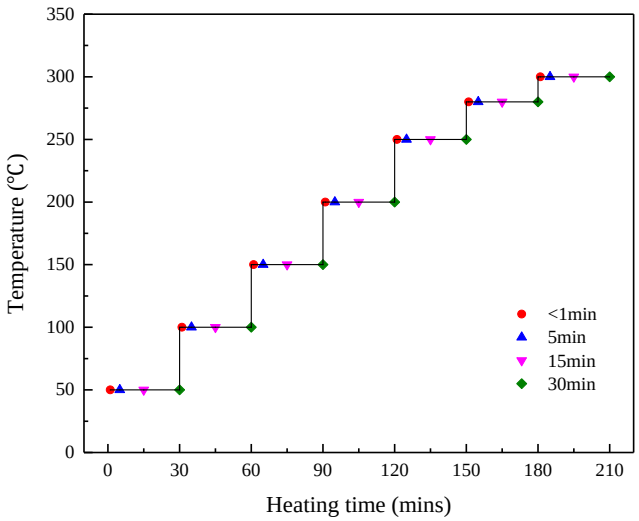

Fig.4 Scheme for studying thermal stability of the passive film in UHV as a function of temperature and heating time (The color symbols on each temperature step indicate the time at which ToF-SIMS depth profiles were acquired)

The thermal stability of the passive film in vacuum was studied *in situ* by ToF-SIMS. Fig.4 shows the scheme used for the thermal treatment given to the passive oxide film under UHV in the ToF-SIMS analysis chamber. After passivation of the 316L SS sample (0.4V/SCE in 0.05M H_2SO_4 for 1h), it was introduced in the ToF-SIMS analysis chamber under a base pressure lower than 10^{-9} mbar. The experiments were performed through stepwise heating from 50°C to 300°C with steps of 50°C. The temperature of 280°C was added in the experiments since under relatively high temperature, even slight increase of the temperature could cause modifications of the composition and structure of the passive oxide. After each temperature step, ToF-SIMS depth profiles were acquired for heating times of 1 minute, 5 minutes, 15 minutes and 30 minutes. Each profile was obtained on a new area of the sample surface.

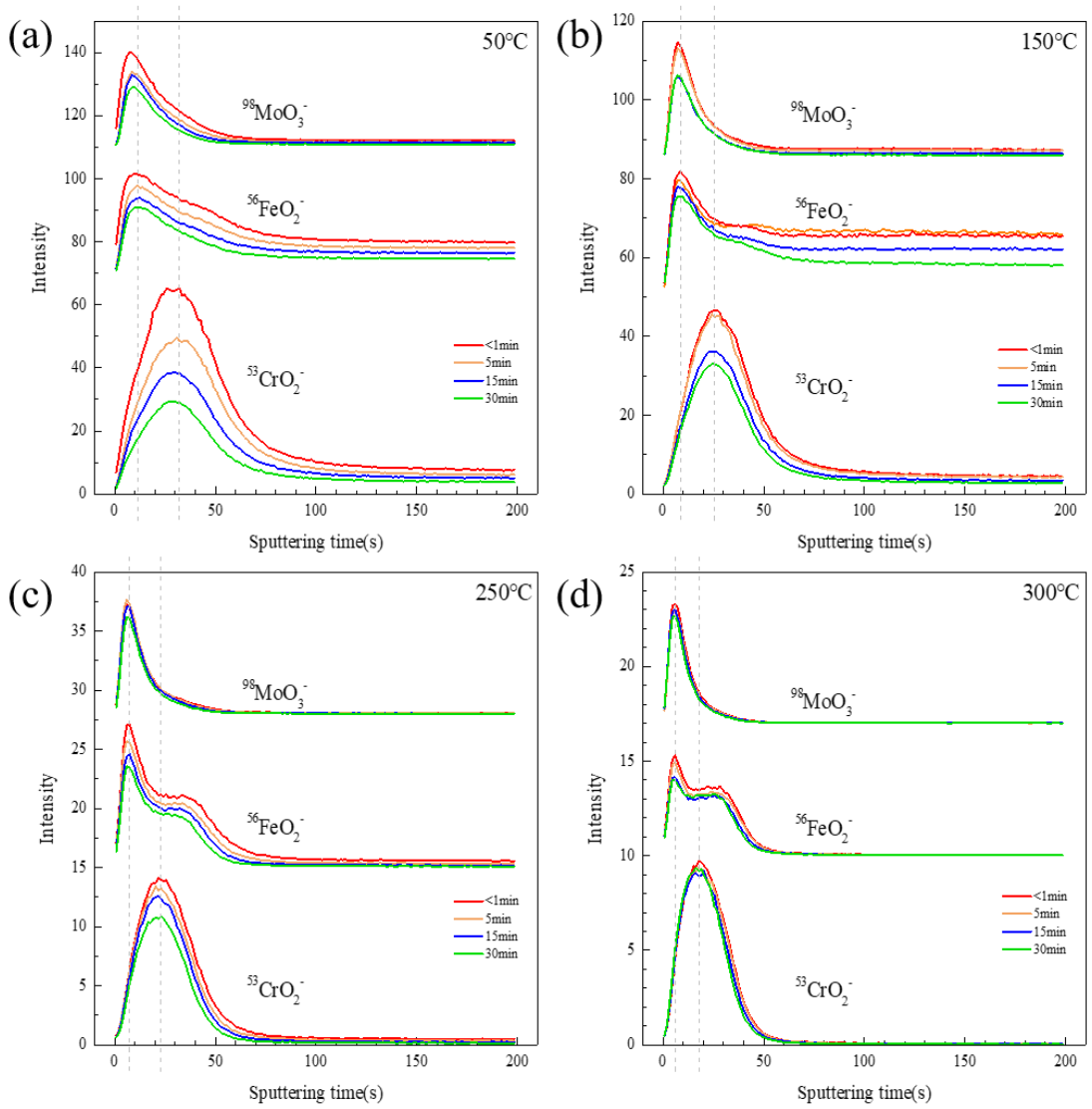

Fig.5 ToF-SIMS depth profiles of $^{53}CrO_2^-$, $^{56}FeO_2^-$ and $^{98}MoO_3^-$ at (a) 50°C, (b) 150°C, (c) 250°C and (d) 300°C for different heating times. (The intensities are normalized by the intensity of Fe_2^- in the substrate)

Fig.5 shows the $^{53}CrO_2^-$, $^{56}FeO_2^-$ and $^{98}MoO_3^-$ ToF-SIMS depth profiles recorded on the passive film heated up to 50°C, 150°C, 250°C and 300°C for different heating times. Although all the temperatures indicated in Fig.4 have been investigated, only the data for these 4 temperatures are discussed here since no strong change occurred on the passive film at the other intermediate temperatures. The depth profiles of Ni_2^- and Fe_2^- ions are not included in Fig.5, since they were unchanged during heat treatment.

As observed in Fig.5(a), when the sample is heated up to 50°C and maintained at this temperature for 1, 5, 15 and 30 min, the shapes of $^{53}CrO_2^-$, $^{56}FeO_2^-$ and $^{98}MoO_3^-$ profiles are not significantly modified as compared with the profile obtained at room temperature. This demonstrates that the native oxide layer is stable at 50°C, with a duplex structure formed by an Fe and Mo rich outer oxide and a Cr rich inner oxide.

Upon heating at 150°C in vacuum, the separation between outer layer composed of Fe oxide ($^{56}FeO_2^-$) and Mo oxide ($^{98}MoO_3^-$) and inner layer composed of Cr oxide ($^{53}CrO_2^-$) is enhanced. The inner oxide/outer oxide interface becomes sharper as shown by the sharper decrease of both the $^{98}MoO_3^-$ and $^{56}FeO_2^-$ signals after heating at 150°C (Fig.5(b)).

At temperatures higher than 200°C, as showed in Fig.5(c) for 250°C and (d) for 300°C, the $^{56}FeO_2^-$ and $^{98}MoO_3^-$ depth profiles show again maxima of intensity located in the outer part of the oxide film. However, for the $^{56}FeO_2^-$ signal, a clear plateau of lower intensity is observed in the inner chromium oxide rich layer and then a sharp decrease when going through the oxide/alloy interface.

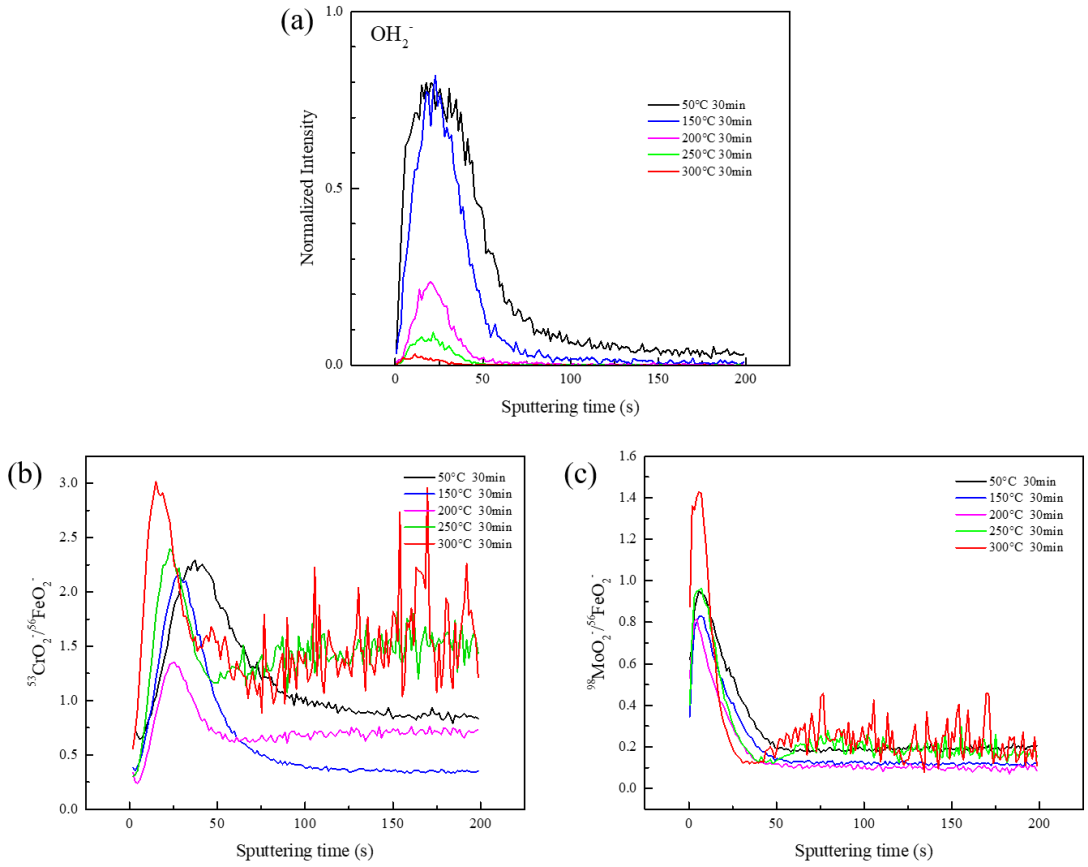

Fig.6 ToF-SIMS depth profiles as function of temperature after 30 mins at each temperature: (a) OH_2^- secondary ion, (b) $^{53}CrO_2^-/^{56}FeO_2^-$ intensity ratio, and (c) $^{98}MoO_2^-/^{56}FeO_2^-$ intensity ratio. (In (a), the intensity is normalized by the intensity of Fe_2^- in the substrate)

Although the $^{53}CrO_2^-$ depth profiles remain high in the inner part of the oxide film, the intensity ratio between the $^{53}CrO_2^-$ and $^{56}FeO_2^-$ in the inner oxide region (taken around 40s of sputtering on Fig 6(b)), is decreasing from 2.3 at 50°C to 1.3 with increasing the temperature up to 200°C. The modification of the $^{53}CrO_2^-/^{56}FeO_2^-$ ratio demonstrates the modification of the inner oxide layer. To understand this evolution, one also have to look at the OH_2^- species. Fig 6(a) shows the ToF-SIMS depth profiles of the OH_2^- species as function of temperature. The intensity maxima of the OH_2^- signal remarkably drop from 0.8 at 50°C to 0.2 at 200°C. The composition of the passive film formed in 0.05M H_2SO_4(aq) has already been studied by Maurice and Marcus [6, 21]. It was shown that the passive film formed at room temperature contains 6% of iron hydroxide, 23% of chromium hydroxide, and about 10% of water ligand. Thus, the evolution of OH_2^- is assigned to the decomposition of hydroxides and dehydration. The decreasing of the $^{53}CrO_2^-/^{56}FeO_2^-$ ratio in the inner oxide with increasing temperature is assigned mainly to the decomposition of Cr hydroxide (a major constituent of the inner oxide at low temperature) yielding Cr oxide.

Although dehydroxylation and dehydration have been showed this effect cannot explain the modification of the $^{56}FeO_2^-$ and $^{53}CrO_2^-$ depth profiles and the sharpness of the inner oxide/outer oxide interface. Looking more precisely at the $^{53}CrO_2^-/^{56}FeO_2^-$ ratio, one observes that it decreases with increasing temperature up to 200°C. When the temperature is increased over 250°C, the $^{53}CrO_2^-/^{56}FeO_2^-$ ratio increases from 1.3 to 2.4. This indicates that the inner oxide becomes more concentrated in Cr. This effect may be due to the increase of Cr diffusion from the metallic substrate to the passive film. Cr being more reactive towards oxygen, the higher concentration of Cr in the inner part of the oxide is related to the reduction of the Fe oxide to form Cr oxide according to the reaction $Fe_2O_3+2Cr \rightarrow Cr_2O_3+2Fe$. This mechanism is in agreement with the standard free energy of formation (ΔG_{500k}°) of chromium oxide and iron oxide (-1004.265 kJ/mol and -687.720 kJ/mol, respectively[28]), and Ellingham oxidation-reaction plot[29-31]. The bilayer structure of the oxide film becomes more marked with an outer oxide that is almost exclusively comprised of Fe oxide and an inner oxide that is almost exclusively comprised of Cr oxide. This also correlates to the modification of the inner oxide / outer oxide interface that becomes sharper when increasing the temperature. Thus, two effects linked with the increase of the temperature have been shown, the first one, which is the main effect at temperatures lower than 250°C, is the dehydroxylation and dehydration of the oxide film, and the second one, that is the main effect at temperatures over 250°C, is the Fe oxide reduction due to bulk Cr diffusing into the inner part of the oxide.

In Fig.6(c), the $^{98}MoO_3^-/^{56}FeO_2^-$ intensity ratio shows only minor changes up to 250°C. Above 250°C, there is a marked increase of the $^{98}MoO_3^-/^{56}FeO_2^-$ intensity ratio, from 0.9 at 250°C up to 1.4 at 300°C. This is also assigned to the formation of molybdenum oxide and reduction of iron oxide. This is similar to the formation of chromium oxide but at higher temperature. This effect is assigned to molybdenum diffusing from the metallic substrate and being oxidised at the expense of iron oxide.

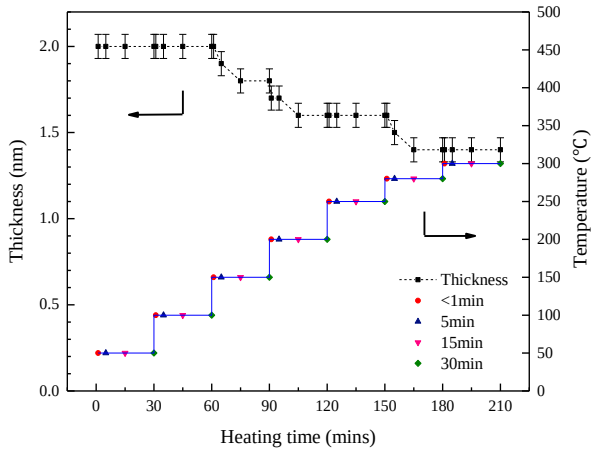

Fig.7 The thickness of the passive film as a function of heating temperature and time

Fig.7 shows the changes of the passive film thickness as a function of heating temperature and time. The passive film thickness remains constant at 2 nm up to 100°C. At higher temperature (up to 250°C), the passive film thickness gradually decreases to 1.6 nm. This change is assigned to the decomposition of the hydroxide and removal of water ligands present after passivation in sulphuric acid. According to the density of chromium oxide and iron oxide (5.22 g/cm^3 and 5.24 g/cm^3), and those of chromium hydroxide and iron hydroxide (3.11 g/cm^3 and 3.4 g/cm^3), the decomposition of hydroxide to oxide will result in a denser and thinner film as observed on Fig.7. Above 200°C, the passive film composition and structure seem more stable, as indicated by the very limited change in oxide film thickness in the 200°C - 300°C (from 1.6 nm to 1.4 nm). This slight film modification in this temperature range is related to the formation of chromium and molybdenum oxide, and reduction of iron oxide. According to the density of Mo(IV) oxide (4.67 g/cm^3), Cr oxide and Fe oxide, the formation of Mo oxide and reduction of Fe oxide will lead to a denser film. In addition, the formation of Mo oxide will consume more Fe oxide due to its higher stoichiometry.

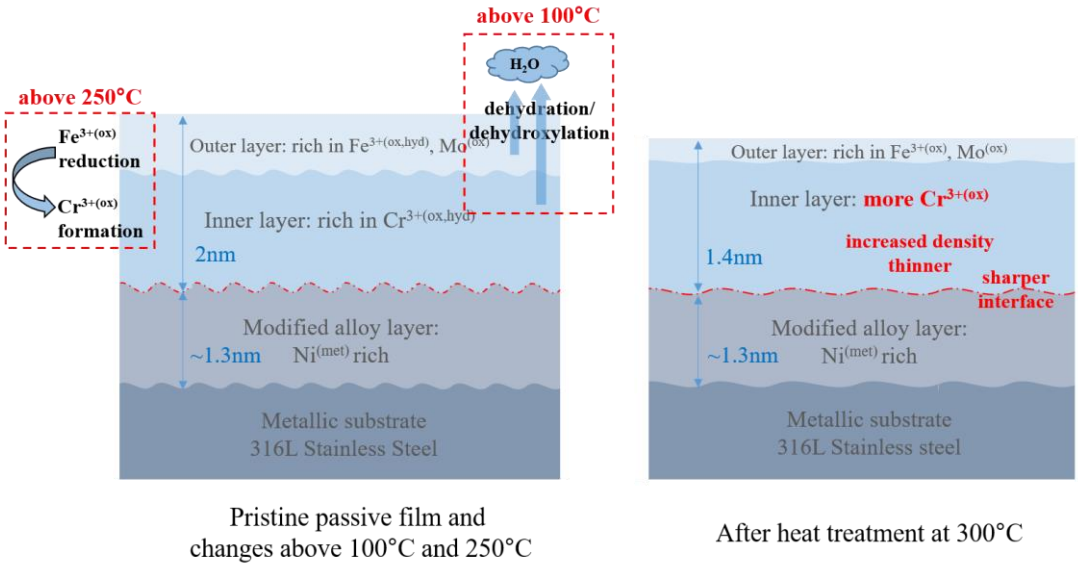

Fig.8 Model for the passive film evolution during UHV heat treatment

According to the results above, a model for the evolution of the passive film formed on 316L SS during step by step heat treatment in UHV is proposed in Fig.8.

After heat treatment at 300°C, the outer layer of the passive film is rich in iron oxide, with a small amount of molybdenum oxide. The inner part of the passive film is mainly comprised of chromium oxide. The interface between the outer and inner oxide layer becomes sharper compared to the film formed at room temperature.

Conclusion

The thermal stability of the passive film formed on 316L stainless steel surface in 0.05M H_2SO_4(aq) at 0.4V/SCE has been investigated through step by step heating in UHV up to 300°C by means of ToF-SIMS. The pristine passive film on the 316L stainless steel presents a bilayer structure. The outer layer is enriched in iron oxide and molybdenum oxide while the inner layer is rich in chromium oxide. The interface between these outer and inner layers is not sharp, meaning that some iron oxide is distributed in the inner region.

At temperatures below 100°C, the passive film is stable and the composition is not modified. At heating temperatures higher than 100°C, the inner oxide/outer oxide interface of the passive film stars to become sharper. The temperature of 250°C is a critical point. In the temperatures range between 100°C and 250° C, the main change in the passive film is the decomposition of hydroxide (mainly the Cr hydroxide) and removal of the water ligands, giving a higher chromium oxide content. At temperatures above 250°C, the main change on the passive film is the reduction of Fe oxide caused by bulk Cr diffusing into the inner part of the oxide. The thickness of the passive film (2 nm) is not changed at heating temperatures up to 100°C. Then, at higher temperature (up to 250°C), the passive film thickness gradually decreases to 1.6 nm, which corresponds to the dehydroxylation and dehydration of the oxide film. Very limited change in the film thickness is observed at temperatures higher than 250°C (from 1.6 nm to 1.4 nm). This slight film modification in this temperature range is assigned to the formation of chromium and molybdenum oxide, and reduction of iron oxide.

The passive film, after stepwise heating in UHV, still exhibits a bilayer comprising Fe oxide and Mo oxide in the outer film, and Cr oxide in the inner part. The content of Cr oxide in the film becomes higher than in the pristine passive film. The interface between the outer and inner oxide layer becomes sharper compared to the film formed at room temperature.

Acknowledgements

This project has received funding from the European Research Council (ERC) under the European Union's Horizon 2020 research and innovation program (ERC Advanced grant no. 741123). Région île-de-France is acknowledged for partial funding of the ToF-SIMS equipment. China Scholarship Council (CSC) is acknowledged for the scholarship to the first author (No. 201706460018).

Data availability statement

The datasets generated for this study are available on request to the corresponding author.

References

[1] V. Maurice, P. Marcus, Progress in corrosion science at atomic and nanometric scales, Prog. Mater. Sci. 95 (2018) 132-171.

[2] V. Maurice, P. Marcus, Current developments of nanoscale insight into corrosion protection by passive oxide films, Curr. Opin. Solid State Mater. Sci. 22 (2018) 156-167.

[3] V. Maurice, W. Yang, P. Marcus, X- Ray Photoelectron Spectroscopy and Scanning Tunneling Microscopy Study of Passive Films Formed on (100) Fe- 18Cr- 13Ni Single- Crystal Surfaces, J. Electochem. Soc. 145 (1998) 909-920.

[4] V. Maurice, W. Yang, P. Marcus, XPS and STM Study of Passive Films Formed on Fe- 22Cr (110) Single- Crystal Surfaces, J. Electochem. Soc. 143 (1996) 1182-1200.

[5] Z. Feng, X. Cheng, C. Dong, L. Xu, X. Li, Passivity of 316L stainless steel in borate buffer solution studied by Mott–Schottky analysis, atomic absorption spectrometry and X-ray photoelectron spectroscopy, Corros. Sci. 52 (2010) 3646-3653.

[6] Z. Wang, F. Di-Franco, A. Seyeux, S. Zanna, V. Maurice, P. Marcus, Passivation-induced physicochemical alterations of the native surface oxide film on 316L austenitic stainless steel, J. Electochem. Soc. 166 (2019) C3376-C3388.

[7] N.E. Hakiki, Comparative study of structural and semiconducting properties of passive films and thermally grown oxides on AISI 304 stainless steel, Corros. Sci. 53 (2011) 2688-2699.

[8] Č. Donik, A. Kocijan, J.T. Grant, M. Jenko, A. Drenik, B. Pihlar, XPS study of duplex stainless steel oxidized by oxygen atoms, Corros. Sci. 51 (2009) 827-832.

[9] R.K. Wild, High temperature oxidation of austenitic stainless steel in low oxygen pressure, Corros. Sci. 17 (1977) 87-104.

[10] I. Saeki, H. Konno, R. Furuichi, T. Nakamura, K. Mabuchi, M. Itoh, The effect of the oxidation atmosphere on the initial oxidation of type 430 stainless steel at 1273 K, Corros. Sci. 40 (1998) 191-200.

[11] N.E. Hakiki, M.F. Montemor, M.G.S. Ferreira, M. da Cunha Belo, Semiconducting properties of thermally grown oxide films on AISI 304 stainless steel, Corros. Sci. 42 (2000) 687-702.

[12] L. Ma, F. Wiame, V. Maurice, P. Marcus, New insight on early oxidation stages of austenitic stainless steel from in situ XPS analysis on single-crystalline Fe–18Cr–13Ni, Corros. Sci. 140 (2018) 205-216.

[13] S.C. Tjong, J. Eldridge, R.W. Hoffman, EAS studies of the oxides formed on iron-chromium alloys at 400°C, Applic. Surf. Sci. 14 (1983) 297-306.

[14] T.J. Driscoll, P.B. Needham, The oxidation of Fe-Cr surface and bulk alloys at 300°C, Oxid. Met. 13 (1979) 283-298.

[15] L.Q. Guo, M. Li, X.L. Shi, Y. Yan, X.Y. Li, L.J. Qiao, Effect of annealing temperature on the corrosion behavior of duplex stainless steel studied by in situ techniques, Corros. Sci. 53 (2011) 3733-3741.

[16] L. Zhang, W. Zhang, Y. Jiang, B. Deng, D. Sun, J. Li, Influence of annealing treatment on the corrosion resistance of lean duplex stainless steel 2101, Electrochim. Acta 54 (2009) 5387-5392.

[17] G. Bombara, A. Alderisio, U. Bernabai, M. Cavallini, The effects of heating in a vacuum on the surface properties of a low chromium stainless steel, Surf. Technol. 14 (1981) 17-23.

[18] R.L. Park, J. Houston, D. Schreiner, Chromium depletion of vacuum annealed stainless steel surfaces, J. Vac. Sci. Technol. 9 (1972) 1023-1027.

[19] R.K. Wild, Vacuum annealing of stainless steel at temperatures between 770 and 1470K, Corros. Sci. 14 (1974) 575-586.

[20] P. Konarski, K. Kaczorek, J. Senkara, Effects of vacuum heating in AISI 410 and AISI 321 stainless steels' surface layer revealed by SIMS/GDMS depth profile analysis, Surf. Interface Anal. 43 (2011) 217-220.

[21] V. Maurice, H. Peng, L.H. Klein, A. Seyeux, S. Zanna, P. Marcus, Effects of molybdenum on the composition and nanoscale morphology of passivated austenitic stainless steel surfaces, Faraday Discuss. 180 (2015) 151-170.

[22] E. Gardin, S. Zanna, A. Seyeux, A. Allion-Maurer, P. Marcus, Comparative study of the surface oxide films on lean duplex and corresponding single phase stainless steels by XPS and ToF-SIMS, Corros. Sci. 143 (2018) 403-413.

[23] P. Marcus, V. Maurice, Investigations of Structure and Stability of Passive Films by Surface Analytical Techniques, Elsevier, Oxford, 2018, pp. 259-266.

[24] E. Gardin, S. Zanna, A. Seyeux, A. Allion-Maurer, P. Marcus, XPS and ToF-SIMS characterization of the surface oxides on lean duplex stainless steel – Global and local approaches, Corros. Sci. 155 (2019) 121-133.

[25] K. Asami, K. Hashimoto, S. Shimodaira, Changes in the surface compositions of FeCr alloys caused by heating in a high vacuum, Corros. Sci. 18 (1978) 125-137.

[26] J.E. Castle, R. Ke, J.F. Watts, Additional in-depth information obtainable from the energy loss features of photoelectron peaks: the oxidation and reduction of an Fe/Cr alloy in oxygen at low partial pressures and ultra high vacuum, Corros. Sci. 30 (1990) 771-798.

[27] S. Bouhieda, F. Rouillard, V. Barnier, K. Wolski, Selective Oxidation of Chromium by O2 Impurities in CO2 During Initial Stages of Oxidation, Oxid. Met. 80 (2013) 493-503.

[28] I. Barin, Thermochemical data of pure substances, VCH, (1989).

[29] F. Richardson, The Thermodynamics of Substances of Interest in Iron and Steel Making from 0℃ to 2400℃ I-Oxides, J. Iron Steel Inst. 160 (1948) 261-270.
[30] H.J.T. Ellingham, Reducibility of oxides and sulfides in metallurgical processes, J. Soc. Chem. Ind. 63 (1944) 125-133.
[31] T. Ohmi, Y. Nakagawa, M. Nakamura, A. Ohki, T. Koyama, Formation of chromium oxide on 316L austenitic stainless steel, J. Vac. Sci. Tech. A: Vac. Surf. Films 14 (1996) 2505-2510.